RECLAMATION

*Managing Water in the West*

**Report DSO-07-03**

# Problems Encountered from the Use (or Misuse) of Rayleigh Damping

## Dam Safety Technology Development Program

**U.S. Department of the Interior**
**Bureau of Reclamation**
**Technical Service Center**
**Denver, Colorado**

**December 2007**

# Problems encountered from the use (or misuse) of Rayleigh damping

John F. Hall [*,†]

*Department of Civil Engineering, Caltech, Pasadena CA*

## SUMMARY

Rayleigh damping is commonly used to provide a source of energy dissipation in analyses of structures responding to dynamic loads such as earthquake ground motions. In a finite element model, the Rayleigh damping matrix consists of a mass-proportional part and a stiffness-proportional part; the latter typically uses the initial linear stiffness matrix of the structure. Under certain conditions, for example, a nonlinear analysis with softening nonlinearity, the damping forces generated by such a matrix can become unrealistically large compared to the restoring forces, resulting in an analysis being unconservative. Potential problems are demonstrated in this paper through a series of examples. A remedy to these problems is proposed in which bounds are imposed on the damping forces.

KEY WORDS: Rayleigh damping; nonlinear dynamic analysis; earthquake ground motion

[*] Correspondence to: John F. Hall, Department of Civil Engineering, Mail Code 104-44, California Institute of Technology, Pasadena, CA

[†] E-mail: johnhall@caltech.edu

# INTRODUCTION

Numerical models of vibrating structures account for three sources of energy dissipation through nonlinear restoring forces, energy radiation, and damping in the structure. In most applications, energy dissipation is desirable since it reduces the level of response. Since too much energy dissipation can be unconservative, accurate representation in a model is important.

Knowledge of energy dissipation comes mainly from laboratory testing of structural components and materials, system identification using time history records of structural response, and field testing with portable shaking machines. Laboratory test data tends to be very specific and can be translated directly into nonlinear restoring force models, such as elastic-plastic hysteretic behavior. System identification results are generally much less specific in that all three sources of energy dissipation may be present, and seldom can characteristics of the individual sources be separated out. Field vibration testing is usually always performed at low amplitude levels, and so the determined damping values would contain only contributions from energy radiation and damping in the structure. This data is useful for calibrating numerical models in the low-amplitude range, but again, the relative amounts of these two mechanisms of energy dissipation are not generally determined. The same can be said of those system identification studies that examine low-amplitude records, including ambient data.

Given the nature of the available data, a logical procedure to calibrate the energy dissipation features of a numerical model would be to include appropriate energy radiation mechanisms such as energy absorbing foundation elements or transmitting boundaries, and then provide enough damping in the structure to match the low-amplitude field test or system identification data. For higher levels of response, nonlinear restoring force models based on laboratory tests would be added, which would act together with the previously defined energy radiation and structural damping mechanisms. Sometimes, for simplicity, the energy radiation components could be omitted; then the low-amplitude calibration would be done only with the damping in the structure.

Numerical models almost always represent damping in the structure as the linear viscous type. Although an approximation, this type of damping is mathematically convenient. In the equation of motion, linear viscous damping takes the form of a damping matrix of constant coefficients multiplying a vector of velocities of the degrees of freedom. The calibration exercise consists of choosing the coefficients so that amounts of modal damping consistent with the data are produced for modes of the linear system. However, such calibration is not always sufficient to guarantee that the effects of linear viscous damping will be reasonable. Of course, in a standard linear analysis, viscous damping must behave predictably because of the modal nature of linear response and the association of the damping matrix with modal damping values. In other cases, problems can occur. Typical users of commercial finite element programs may not be aware of these potential problems because damping forces are seldom included in a

program's output. Nor would effects on the results that are included in a program's output necessarily be evident.

The next section gives background on Rayleigh damping, which is the particular form of linear viscous damping considered in this paper. The main body of the paper presents examples where Rayleigh damping is shown to generate unrealistically high damping forces. Each example is accompanied by a discussion of what goes wrong, and sometimes possible remedies are suggested. Then, a capped viscous damping formulation is introduced that can overcome some of the problems described.

## RAYLEIGH DAMPING

Of interest in this paper are those cases where for various reasons, such as the presence of nonlinear restoring forces, the matrix equation of motion of a structure must be solved directly, rather than the uncoupled modal equations. The matrix equation of motion takes the form [1]

$$[M]\{\ddot{x}(t)\} + [C]\{\dot{x}(t)\} + \{R_s(t)\} = \{F_{stat}\} + \{F_{dyn}(t)\} \qquad (1)$$

where $\{x(t)\}$ contains the displacement degrees of freedom (translations and rotations) as a function of time *t*, an over dot denotes a time derivative, $[M]$ is the mass matrix, $[C]$ is the damping matrix, $\{R_s(t)\}$ is the vector of restoring forces (forces and moments), $\{F_{stat}\}$ is the static load vector, and $\{F_{dyn}(t)\}$ is the dynamic load vector. Linear viscous damping in the structure is assumed, and $[C]$ could contain energy radiation terms. However, this paper focuses on Rayleigh damping, in which case $[C]$ is expressed as

$$[C] = a_M[M] + a_K[K] \qquad (2)$$

where $a_M$ and $a_K$ are constants with units of $s^{-1}$ and *s*, respectively, and $[K]$ is the linear stiffness matrix of the structure constructed with initial tangent stiffnesses. Thus, $[C]$ consists of a mass-proportional term and a stiffness-proportional term. This choice of $[K]$ in the stiffness-proportional damping term may be the only option offered by a commercial finite element program.

The procedure for determining $a_M$ and $a_K$ involves imparting appropriate values of damping, to the degree possible, to the modes of the linear system, which is represented by equation (1) except that the restoring forces are given by

$$\{R_s(t)\} = [K]\{x(t)\}. \qquad (3)$$

Damping of mode *i* is quantified by the damping ratio $\xi_i$, the ratio of the mode's damping to the critical value [2]. If $a_M$ and $a_K$ are known, $\xi_i$ can be found from

$$\xi_i = \frac{1}{2\omega_i} a_M + \frac{\omega_i}{2} a_K \qquad (4)$$

where $\omega_i$ is the natural frequency (*rad/s*) of mode *i*. Thus, $a_M$ and $a_K$ can be set to give any damping ratio to any two modes. Other modes will receive default amounts of damping that can be computed from equation (4).

The following procedure is convenient for determining $a_M$ and $a_K$. Select a desired amount of damping $\xi$ and a frequency range from $\hat{\omega}$ to $R\hat{\omega}$ covering those modes important to the response, where $R > 1$. Compute $\Delta$ from

$$\Delta = \xi \frac{1 + R - 2\sqrt{R}}{1 + R + 2\sqrt{R}} \qquad (5)$$

where $\Delta$ determines bounds on the damping ratios that are imparted to those modes within the specified frequency range. Any such mode will have a damping ratio bounded by $\xi_{\max} = \xi + \Delta$ and $\xi_{\min} = \xi - \Delta$. If these bounds are satisfactorily narrow, the constants $a_M$ and $a_K$ are then found from

$$a_M = 2\xi\hat{\omega} \frac{2R}{1 + R + 2\sqrt{R}} \qquad (6a)$$

$$a_K = 2\xi \frac{1}{\hat{\omega}} \frac{2}{1 + R + 2\sqrt{R}} \qquad (6b)$$

and can be used to compute an actual damping value $\xi_i$ for mode *i* from equation (4) if $\omega_i$ is known. Figure 1 shows that $\xi_i = \xi_{\max}$ if $\omega_i = \hat{\omega}$ or $\omega_i = R\hat{\omega}$, and that $\xi_i = \xi_{\min}$ if $\omega_i = \sqrt{R}\hat{\omega}$. If $\omega_i$ is outside the range $\hat{\omega}$ to $R\hat{\omega}$, then $\xi_i > \xi_{\max}$. Above $R\hat{\omega}$, $\xi_i$ increases with $\omega_i$, approaching a linear relation as the last term in equation (4) dominates.

Having a small $\Delta$ (relative to $\xi$) and a large *R* are desirable but, as is evident from equation (5), competing goals. If for a given *R* the value of $\Delta$ from equation (5) is unacceptably large, then *R* must be reduced. Some compromise will usually have to be made. Consider an example to illustrate what can be achieved. Suppose the fundamental frequency $\omega_1$ of a building is expected to shorten to $\frac{2}{3}\omega_1$ due to nonlinear softening. Then $\hat{\omega}$ can be set to $\frac{2}{3}\omega_1$. If the building behaves like a shear beam in its linear range, then its second-mode frequency $\omega_2$ equals $3\omega_1$. To cover the frequency range from $\frac{2}{3}\omega_1$

to $3\omega_1$, $R$ is set to 4.5. This gives $\Delta$ from equation (5) as $0.129\xi$. Thus, if $\xi$ = 0.05, then $\xi_{\max}$ = 0.056 and $\xi_{\min}$ = 0.044, which are reasonably narrow bounds. If mode 3 has frequency $\omega_3$ equal to $5\omega_1$, its damping would be higher at $\xi_3$ = 0.083, as computed from equations (4) and (6).

The above procedure aims to achieve a near constant value of damping for all modes whose frequencies $\omega_i$ fall in the range from $\hat{\omega}$ to $R\hat{\omega}$. This is consistent with much field data, which indicates modal damping ratios are fairly constant for a given structure. In general, civil engineering structures are lightly damped, with modal damping ratios seldom exceeding 0.10 and sometimes as low as 0.01 or 0.02.

Other formulations of the linear viscous damping matrix are available that offer greater control over the damping ratios imparted to the modes [2]. However, these $[C]$ matrices are full; they lack the sparse and banded features of $[K]$ and $[M]$. Thus, their presence greatly increases the computational effort required to integrate the matrix equation of motion. For this reason, they are seldom used. With Rayleigh damping, sparseness and bandedness are imparted to $[C]$ since it is the scaled sum of $[M]$ and $[K]$.

Another feature of Rayleigh damping is that $[C]$ has a simple physical interpretation [3]. If $[M]$ is a diagonal matrix (often the case or can be made so with good approximation), then the diagonal coefficients of $a_M[M]$ are mass-proportional damping constants for a set of linear viscous dampers that connect each degree of freedom to a fixed support. The coefficients of $a_K[K]$ are stiffness-proportional damping constants for a set of linear viscous dampers that interconnect the degrees of freedom in an arrangement "parallel" to the structural stiffness.

The terms $a_M[M]$ and $a_K[K]$ can be viewed as originating from rate-dependent additions to the equations of elasticity that provide damping. The momentum and constitutive relations [4] are augmented as follows:

$$\frac{\partial \sigma_{ij}}{\partial x_i} + X_i = \rho \ddot{u}_i + a_M \rho \dot{u}_i \qquad (7)$$

$$\sigma_{ij} = K_{ijkl}\varepsilon_{kl} + a_K K_{ijkl}\dot{\varepsilon}_{kl} \qquad (8)$$

where $\sigma$, $\varepsilon$ and $K$ are stress, strain and elasticity tensors, respectively, $x$ is spatial coordinate, $X$ is body force, $\rho$ is mass density, $u$ is displacement, and $i$, $j$, etc. denote directions in a rectangular coordinate system. Upon application of finite element discretization procedures, the $a_M \rho \dot{u}_i$ term ends up as $a_M[M]\{\dot{x}(t)\}$, and the $a_K K_{ijkl}\dot{\varepsilon}_{kl}$ term ends up as $a_K[K]\{\dot{x}(t)\}$.

The augmented constitutive relation (8) represents a form of viscoelasticity known as a Voigt solid [4] and is a valid type of material model. However, the augmented momentum equation is invalid because the $a_M \rho \dot{d}$ term represents the effects of a viscous, penetrating ether in which the structure is immersed. Even though this mass-proportional part of Rayleigh damping can not exist for an actual structure, it is still widely used in finite element practice because of the additional control it provides over the modal damping ratios.

The simple physical interpretation of the Rayleigh damping matrix serves as a general tool that can be used to assess the effects of the damping and the size of the damping forces. For a linear structure, modal concepts are also available for this purpose using the modal damping ratios. However, modal damping ratios may not always be a suitable tool, such as when Rayleigh damping is being applied in a nonstandard way or when the restoring forces are nonlinear. In such cases, the question arises as to whether the damping forces generated by the $a_M [M]$ and $a_K [K]$ terms are reasonable. The following section presents some examples from earthquake engineering to illustrate problems that can arise.

## EXAMPLES

### *Earthquake Formulation*

This first example has to do with the way in which earthquake excitation is included in the equation of motion of a structure. For simplicity, the interaction between the structure and its foundation or supporting medium is neglected; the earthquake ground motion is assumed to be spatially uniform; and only one horizontal component is considered. This simple case is sufficient to describe how Rayleigh damping can have different effects depending on how the earthquake excitation is formulated.

One method to apply the earthquake loading is to specify the earthquake motions at the base of the structure. A convenient way to do this, which can be accommodated by most commercial computer programs, is to attach a large artificial mass $m_b$ to each node at the base of the structure and apply to each of the horizontal degrees of freedom in the direction of the ground motion a horizontal force

$$F_{eq}(t) = m_b \ddot{x}_{eq}(t) \qquad (9)$$

where $\ddot{x}_{eq}(t)$ is the ground acceleration time history. The vector $\{F_{dyn}(t)\}$ in equation (1) would be comprised of such forces. Typically, the total artificial mass added to the base would be at least $10^3$ to $10^4$ times the total mass of the structure. The formulation is depicted in Figure 2a which also shows the mass-proportional and stiffness-proportional damping mechanisms.

Ideally, the role of damping in a structure under earthquake excitation should be to damp the vibrational motion of the structure relative to its base motion. As seen in Figure 2a, the mass-proportional dampers, being connected to fixed supports, damp the total motion of the structure. A better arrangement would be for these dampers to connect to a frame that moves with the base of the structure. To accomplish this in the equation of motion, express the total motion of the structure $\{x(t)\}$ as the sum of a rigid part moving with the base and a part relative to the base:

$$\{x(t)\} = \{r\}x_{eq}(t) + \{x_{rel}(t)\} \qquad (10)$$

where $\{r\}$ is a vector of 1's in positions corresponding to horizontal degrees of freedom in the direction of the ground motion and 0's elsewhere. Substitution into equation (1) gives

$$[M]\{\ddot{x}_{rel}(t)\} + [C]\{\dot{x}_{rel}(t)\} + \{R_s(t)\} = \{F_{stat}\} - [M]\{r\}\ddot{x}_{eq}(t) \qquad (11)$$

where a term $[C]\{r\}\dot{x}_{eq}(t)$ has been discarded. Omitting this term is equivalent to reconnecting the mass-proportional dampers to a frame moving with the base. (Note that $[C]\{r\}$ equals $a_M[M]\{r\}$ since $\{r\}$ is a rigid body motion.) See Figure 2b.

Equation (11) is a standard earthquake loading formulation [2] and is implemented in some commercial finite element computer programs. It is an alternative to equations (1) and (9) and is preferred because it excludes the extraneous damping forces $a_M[M]\{r\}\dot{x}_{eq}(t)$. To demonstrate the potential significance of these forces, take $\hat{\omega} =$ (1400 *m*/*s*)/*H*, $\xi$ = 0.10, and *R* = 4.5 as for the concrete gravity dam example presented later, where *H* is the height of the dam and $\xi$ is the desired damping ratio. With $H = 100$ *m*, $a_M$ is computed as $2.6\,s^{-1}$ from equation (6a). The peak for the ground velocity $\dot{x}_{eq}(t)$ is chosen as 100 *cm*/*s*, which is on the high side but not an upper bound. With these values, the extraneous damping forces are evaluated as $[M]\{r\} \cdot 260\,cm/s^2$, which would not likely be negligible. However, the extraneous damping forces would be smaller for more lightly damped structures or for ones with a lower fundamental frequency $\omega_1$ (giving a lower value of $\hat{\omega}$).

Another issue with the mass-proportional damping term arises with the formulation of equations (1) and (9). The large base masses $m_b$ should not be included in the mass matrix $[M]$ when it is used to compute the $a_M[M]$ part of the damping matrix $[C]$. Otherwise, the forces $F_{eq}(t)$ in equation (9) need to be augmented as

$$F_{eq}(t) = m_b\ddot{x}_{eq}(t) + a_M m_b \dot{x}_{eq}(t) \qquad (12)$$

to obtain the correct base motion. To demonstrate the potential importance of the last term in equation (12), again take $a_M$ as $2.6\,s^{-1}$ and the peak for $\ddot{x}_{eq}(t)$ as 100 *cm*/*s*. With these values, the last term in equation (12) is evaluated as $m_b \cdot 260\ cm/s^2$, which indicates that the imposed base acceleration of the structure would be significantly in error if the last term were omitted. This error would be smaller for lighter damping or a lower $\omega_1$.

Examples in the following sections use the earthquake formulation in terms of relative motion, i.e., equation (11). This avoids the potential problems discussed above.

*10-Story Building*

In this example, a 10-story building (Figure 3) is subjected to an actual ground motion record (Figure 4). The building's stiffness is modeled with a bilinear shear spring in each story, the ratio of post-yield stiffness to initial stiffness being 0.03. Initial stiffnesses $k_j$ of the springs are proportional to the story values shown in Figure 3 and are scaled to give the building a fundamental period $T_1$ of 1.4 seconds, all floor masses being taken as equal. The yield strengths $R_{sy,j}$ of the springs are also proportional to the same story values and are scaled so that the first-story spring has a yield strength of 0.12 times the weight *W* of the building; $W = 10\ mg$, where *m* = floor mass and *g* = gravitational acceleration. This is a reasonable strength for Zone 4 seismic design and includes a significant margin above typical code requirements. The shear spring in each story has the same yield displacement of 1.1 *cm*.

Rayleigh damping is employed using the following parameters: $\hat{\omega} = \frac{2}{3}(2\pi / T_1)$ to account for some drop in $\omega_1$ due to nonlinear softening, $\xi$ = 0.05, and *R* = 4.5. The $a_K[K]$ term is computed using the initial spring stiffnesses which, as mentioned earlier, is how many commercial computer programs operate.

Shown in Figures 5 and 6 are comparisons of time histories of the shear-spring force in the first story and the total damping force on the building. These are consistent quantities to be compared since the shear-spring force in the first story represents the total restoring force acting on the building. The total damping force is found by adding the damping force in the first story, computed as $a_K k_1 \dot{x}_{1,rel}(t)$, to the external damping force on the building, computed by summing the $a_M[M]\{\dot{x}_{rel}(t)\}$ forces.

For the results in Figure 5, the ground acceleration history is scaled down to a peak acceleration of 0.15 *g* so that the response of the building just remains in the linear range. On average, the ratio of peaks in the total damping force to peaks in the first-story spring force is about 9%. This is as expected since, in the present case, the building vibrates primarily in its fundamental mode and frequency. Theoretically, for such vibration the ratio of these forces is $2\xi_1$, which is 0.092 for this 10-story building.

When the full-scale ground acceleration is applied (Figure 6), significant yielding takes place, and the ratio of the peak total damping force to the peak first-story spring force is 46%. In terms of the building's weight, the peak total damping force is $0.072W$, which equals 60% of the yield strength of the building ($0.12W$). No conceivable mechanism in an actual building exists that could produce a damping force this high relative to the strength of the building. Such large damping forces mean the results of the analysis are unconservative.

The situation still exists if mass-proportional damping only is used ($a_K = 0$, $a_M = 2\xi\hat{\omega}$) or if stiffness-proportional damping only is used ($a_M = 0$, $a_K = 2\xi/\hat{\omega}$). For these two cases, the peak total damping force reaches 29% and 102%, respectively, of the yield strength of the building. The source of the problem is that a yielding mechanism is provided to limit the spring forces, but no such mechanism is used for the damping forces. The linearity assumption on the damping forces means they are always proportional to the velocities, no matter how large they become.

Finally, if the building were modeled as a frame of beam and column elements that are capable of forming plastic hinges to represent nonlinear bending effects, a similar situation to that described above for the building comprised of nonlinear shear springs would be encountered. The plastic hinges would limit the moments that could develop at the ends of the beams and columns, which in turn would limit the shear forces in these elements and to some extent the axial forces. The damping forces and moments, on the other hand, without their own limiting mechanism, could reach unrealistically high values.

*Base-Isolated Building*

Consider a base-isolated building (Figure 7) with fundamental period of the superstructure denoted by $T_S$ (period if base were fixed) and with design period of the isolated building denoted by $T_I$. Suppose $[C]$ is constructed using only the superstructure properties since all energy dissipation associated with the isolators is to be modeled explicitly in the isolator elements. Let $\xi$ denote the desired damping in the superstructure. The frequency $\hat{\omega}$ is chosen as $2\pi/T_S$ since the superstructure is expected to remain linear. The ratio of $T_S$ to $T_I$ is taken as 1 to 5, which is reasonable for a 3 or 4-story superstructure and a typical value of 2.5 seconds for $T_I$.

During vibration from an earthquake, the mass-proportional damping forces $a_M[M]\{\ddot{u}_{rel}(t)\}$ on the superstructure produce a total damping force of

$$R_d^{mp}(t) = a_M M_S v_{S,rel}(t) \qquad (13)$$

where $M_S$ is the mass of the superstructure and $v_{S,rel}(t)$ is the velocity of the superstructure relative to the ground. Equation (13) is a good approximation because, with $T_S = T_I/5$, the entire superstructure can be assumed to move as a rigid body on the

flexible isolators, i.e., as a single degree of freedom. Note that the stiffness-proportional part of $[C]$ does not contribute to the total damping force on the superstructure. From equation (13) the damping value $C_I$ in a single-degree-of-freedom equation of motion for the isolated building is $a_M M_S$, which can also be expressed in the usual way as $2\xi_I \omega_I M_S$, where $\xi_I$ is the resulting damping ratio for the single-degree-of-freedom structure (i.e., the isolated building) and $\omega_I = 2\pi / T_I$. Setting the two expressions for $C_I$ equal to each other and solving for $\xi_I$ gives

$$\xi_I = \tfrac{1}{2} a_M / \omega_I . \qquad (14)$$

Substitution for $a_M$ from equation (6a) and replacing frequencies by periods leads to

$$\xi_I = \xi \frac{2R}{1 + R + 2\sqrt{R}} \frac{T_I}{T_S} . \qquad (15)$$

With $\xi$ = 0.05 for the superstructure, $R$ = 4.5, and $T_S = T_I / 5$ as stated above, the resulting damping ratio $\xi_I$ for the isolated building equals 0.23. This unintentionally high value is completely unrealistic and does not even include any energy dissipation associated with the isolation system. In this case the mass-proportional damping term is the source of the problem, along with the non-standard application of Rayleigh damping as it is used only for the relatively high-frequency superstructure. Unlike the example 10-story building in the previous section, no nonlinearity in the restoring forces is required for the unrealistic damping effect to occur in the base-isolated building.

A possible solution to the problem is to use only stiffness-proportional damping. Suppose this is done, but also the contribution from the isolator stiffness is included when computing the stiffness-proportional damping term $a_K [K]$. Bilinear springs are to be employed for the isolators (Figure 8), where the initial stiffness $k_L$ is $\beta$ times the secant stiffness $k_I$ used in design to achieve the period $T_I$ for the isolated building (idealized as a single-degree-of-freedom structure). It is $k_L$ that is used in $[K]$.

During earthquake vibration, the stiffness-proportional damping exerts a force on the superstructure at the location of the isolators given by

$$R_d^{sp}(t) = a_K k_L v_{S,rel}(t) \qquad (16)$$

where, again, the superstructure is assumed to move as a rigid body and $v_{S,rel}(t)$ is its velocity relative to the ground. For stiffness-proportional damping only, $a_K = 2\xi / \hat{\omega}$, where $\xi$ is the desired damping for the isolated building and $\hat{\omega} = 2\pi / T_I$. The term $a_K k_L$ in equation (16) is the damping value $C_I$ in a single-degree-of-freedom equation

of motion for the isolated building, which also equals $2\xi_I \omega_I M_S$ as before. Equating the two expressions for $C_I$ and solving for $\xi_I$ gives

$$\xi_I = \tfrac{1}{2} a_K k_L \frac{1}{\omega_I} \frac{1}{M_S} . \qquad (17)$$

Substituting for $a_K$ and replacing $\omega_I$ by $(k_I / M_S)^{\frac{1}{2}}$ leads to $\xi_I = \beta\xi$ where $\beta = k_L / k_I$ .

Thus, the actual damping ratio $\xi_I$ for the isolated building, idealized as a single-degree-of-freedom structure, is a factor $\beta$ larger than intended. This does not include additional energy dissipation from hysteresis in the bilinear isolator model (Figure 8). Since $\beta$ could be a factor of three or more [5], the effect is significant. The problem is basically similar to that encountered in the previous section with the 10-story building, although a slightly different interpretation can be offered here. When the isolated building vibrates from the design earthquake, the equivalent linear stiffness of the isolators is the secant stiffness $k_I$, yet the stiffness-proportional damping term $a_K [K]$ is computed with the higher initial stiffness $k_L$. This leads to a damping shear force across the isolators that is too large by the factor $\beta$ relative to the intended damping force. Use of $k_I$ in the $a_K [K]$ damping term would be a better choice.

*Gravity Dam Undergoing Sliding*

Consider a concrete gravity dam of approximately triangular cross-section with height *H* and base length $B = 0.8H$ (Figure 9). Water is represented as added mass that augments the mass of the dam, i.e., $[M] = [M_{dam}] + [M_{wat}]$. A pre-existing horizontal crack, along which the dam can slide, runs through the bottom row of finite elements in the dam mesh. If sliding is not taking place, $d\tau_{xy} = G_c \cdot d\gamma_{xy}$, and during sliding, $\tau_{xy} = \pm\mu\sigma_y$, where $\tau_{xy}$ and $\gamma_{xy}$ are the shear stress and strain associated with the sliding plane, $G_c$ is the shear modulus of concrete, $\sigma_y$ is the vertical stress, and $\mu$ is the coefficient of friction. These relations are enforced at the integration points of the elements, a technique known as the smeared crack method.

Rayleigh damping is employed with both mass and stiffness-proportional damping parts. The desired level of damping is $\xi$ = 0.10, and *R* is chosen as 4.5. The frequency $\hat{\omega}$ is set to $\frac{2}{3}(2\pi / T_1)$ to account for nonlinear softening. The fundamental period $T_1$ of the linear dam-water system is expressed as $(0.003\ s/m) \cdot H$ , consistent with approximate period formulas [6]. A possible value for the sliding velocity $v_{sld}$ along the base crack during an earthquake is 50 *cm/s* based on previous studies [7]; this should not be considered as an upper bound.

The magnitude of the damping force exerted on the dam by the mass-proportional damping term during sliding can be estimated by assuming the dam slides as a rigid body at velocity $v_{sld}$. Thus,

$$R_d^{mp} = a_M M v_{sld} \qquad (18)$$

where *M* is the combined mass of the dam and water taken approximately as

$$M = M_{dam} \cdot \tfrac{3}{2} = \tfrac{1}{2} \cdot HB \cdot \frac{\gamma_c}{g} \cdot \tfrac{3}{2} \qquad (19)$$

where the $\frac{3}{2}$ approximately accounts for the water contribution to the mass, $\gamma_c$ is the unit weight of concrete, and *g* is gravitational acceleration. Substitution of equations (6a) and (19) into equation (18) leads to

$$R_d^{mp} = 3\xi\hat{\omega}\frac{2R}{1+R+2\sqrt{R}}\frac{v_{sld}}{g} \cdot W_{dam} \qquad (20)$$

where $W_{dam}$ is the weight of the dam. Further substitution of the suggested values of $\hat{\omega}$, $T_1$, *R* and $v_{sld}$ gives

$$R_d^{mp} = \frac{20m}{H} \cdot W_{dam}\,. \qquad (21)$$

Thus for a 100 *m* high dam, the damping force would reach 20% of the dam's weight for a sliding velocity of 50 *cm/s*, acting in a direction to oppose the sliding. This can be compared to a frictional force of 70% of the dam's weight if, say, the friction coefficient $\mu$ were 0.70. So, the additional resistance to sliding provided by the mass-proportional damping is moderately significant. Of course, no such additional resistance should be present since, as pointed out earlier, mass-proportional damping can not exist in a real structure.

The damping force of interest from the stiffness-proportional damping term acts along the crack as a shear force during sliding. The magnitude of this force is given by

$$R_d^{sp} = \tau_{d,xy} \cdot B \qquad (22)$$

where the damping shear stress is

$$\tau_{d,xy} = a_K G_c \dot{\gamma}_{xy}\,. \qquad (23)$$

This assumes the stiffness-proportional damping is computed using the initial linear $[K]$ of the dam, i.e., the presence of the base crack is not represented. Substitution of equation (6b) and noting that $\dot{\gamma}_{xy} = v_{sld} / h$ during sliding, where *h* is the height of the bottom row of finite elements in the dam mesh, gives

$$R_d^{sp} = 2\xi \frac{1}{\hat{\omega}} \frac{2}{1+R+2\sqrt{R}} G_c \frac{v_{sld}}{h} B . \qquad (24)$$

Some further modification results in

$$R_d^{sp} = (\tfrac{1}{350}\, s/m) \cdot \xi \frac{2}{1+R+2\sqrt{R}} \frac{G_c}{\gamma_c} \frac{v_{sld}}{h} \cdot W_{dam} \qquad (25)$$

where the previously mentioned expressions for $\hat{\omega}$ and $T_1$ have been used, and *B* has been eliminated using equation (19). Finally, taking $G_c / \gamma_c$ = 400,000 *m*, setting *h* to 5*m*, and substitution of the other suggested values for $\xi$, *R* and $v_{sld}$ gives $R_d^{sp} = 2.3 W_{dam}$. However, such a huge damping force probably would never develop because the sliding velocity would stay small. Regardless, the conclusion is that stiffness-proportional damping can greatly inhibit sliding.

This problem with stiffness-proportional damping is similar to that seen in the previous examples with the 10-story building and the base-isolated building. However, the situation with the concrete gravity dam is more severe because the initial linear shear stiffness of the finite elements containing the crack, which is used in the $a_K[K]$ term, is very high. Obviously, the damping force needs to be limited in some way in order for realistic results to be obtained.

*Gravity Dam Undergoing Cracking*

This example is another demonstration of the problem with stiffness-proportional damping in a nonlinear analysis when the initial linear $[K]$ is used in the $a_K[K]$ term. Consider the formation, opening and closing of cracks in a concrete gravity dam discretized with finite elements. When a crack forms in an element, the stress $\sigma_n$ in the direction normal to the crack is set to zero as long as the crack is open, this condition being enforced at the integration points (smeared crack method). Frictional sliding criteria can also be imposed after a crack forms. The strain rate $\dot{\varepsilon}_n$ associated with opening and closing of the crack generates an opposing damping stress $\sigma_{d,n}$ owing to stiffness-proportional damping. The magnitude of this damping stress is approximately equal to

$$\sigma_{d,n} = a_K E_c \dot{\varepsilon}_n \qquad (26)$$

where $E_c$ is Young's modulus for concrete, and where the coupling terms involving Poisson's ratio have been neglected. Use of the initial linear stiffness in the $a_K[K]$ term is assumed, i.e., the presence of the crack is not represented. In terms of the crack opening/closing velocity $v_{oc}$, $\dot{\varepsilon}_n$ equals $v_{oc}/h$, where *h* is the element dimension in the direction normal to the crack. Based on previous studies [8], a possible value of $v_{oc}$ is 50 *cm/s*, which should not be considered an upper bound.

Using equation (6b), equation (26) is written as

$$\sigma_{d,n} = 2\xi \frac{1}{\hat{\omega}} \frac{2}{1+R+2\sqrt{R}} \frac{E_c}{\sigma_{ten}} \frac{1}{h} v_{oc} \cdot \sigma_{ten} \qquad (27)$$

introducing the tensile strength of concrete $\sigma_{ten}$. Inserting the expressions for $\hat{\omega}$ and $T_1$ from the previous example,

$$\sigma_{d,n} = (\tfrac{1}{700}\, s/m) \cdot \xi \frac{2}{1+R+2\sqrt{R}} \frac{E_c}{\sigma_{ten}} \frac{H}{h} v_{oc} \cdot \sigma_{ten}. \qquad (28)$$

Finally, substituting $\xi$ = 0.10, $R$ = 4.5, $v_{oc}$ = 50 *cm/s*, and taking $E_c/\sigma_{ten}$ = 8000 and $H/h$ = 20, the damping stress $\sigma_{d,n}$ is found as $2.3\,\sigma_{ten}$.

This large value indicates that two significant artificial effects can occur regarding the extent of cracking. First, after the first element along the edge of the dam cracks, the opening of this crack could be restrained enough to falsely impede the propagation of the crack further into the interior of the dam mesh. Second, the tensile damping stresses carried across the crack as it opens could load the adjacent elements above and below the cracked element enough to produce false cracks at these locations. An appropriate limit on the damping stress $\sigma_{d,n}$ would resolve these problems. Damping effects associated with sliding along a crack would have to be dealt with simultaneously.

*Penalty Elements*

Penalty elements are commonly used to impose constraints, such as those involving contact and sliding along interfaces. The simplest such application employs nonlinear axial and shear springs shown in parts a and b of Figure 10. The springs would be oriented normal and tangent, respectively, to the interface at the point of contact or potential contact. The stiffness $k_a$ of the axial spring needs to be high to minimize penetration of the surfaces when in contact, similarly for stiffness $k_s$ of the shear spring to minimize slip when the sliding condition is not met. If the stiffness-proportional damping term $a_K[K]$ is formed using such high stiffness values, then large damping forces would be generated upon separation or sliding, which would greatly restrain further movement between the surfaces.

The effect is similar to that demonstrated previously for base sliding and crack opening/closing of the concrete gravity dam example, only even more severe. If the *h* dimension of a finite element of the dam mesh containing a smeared crack (element width normal to crack) were reduced to a small value, the element would act essentially as a penalty element. As seen in equations (25) and (28), the damping force or stress is inversely proportional to *h*.

Another application of penalty elements is using rotational springs to model plastic hinges in beam elements (Figure 10c). When the moment *M* carried by a spring is less than the plastic moment capacity $M_p$ of the beam, then the rotational stiffness $k_r$ of the spring needs to be high to minimize its contribution to the flexibility of the beam. If such a high stiffness is included in the $a_K[K]$ term, a large damping moment will be generated when *M* reaches $M_p$ and the spring starts to develop a relative rotation, which will then act to greatly restrain further relative rotation.

The simplest solution to the stiffness-proportional damping problem with penalty elements is not to include any stiffness contributions from these elements in the $a_K[K]$ term of the damping matrix. Since penalty elements are present to provide constraints and do not contribute to the elastic deformability of the structure, there is no physical reason why they should contain damping. On the other hand, if some damping is needed, say, to control spurious oscillations, then appropriate limits on the damping forces should be employed to avoid unrealistically high damping forces being generated.

## CAPPED VISCOUS DAMPING

As demonstrated in the previous examples, under certain conditions problems can occur with both the mass and stiffness-proportional parts of Rayleigh damping. In this section, a modified damping formulation is examined in which the mass-proportional contribution is eliminated and the stiffness-proportional contribution is bounded. This is an attempt to overcome the problems that have been discussed.

Consider as an example the simple model used earlier for the 10-story building shown in Figure 3. A capped viscous damper is placed in each story along side the shear spring there. The amplitude of the shear force in the damper in story *j* is computed as

$$R_{d,j}(t) = \pm \min\left(a_K k_j \left|\dot{x}_{rel,j}(t) - \dot{x}_{rel,j-1}(t)\right|, 2\xi R_{sy,j}\right) \qquad (29)$$

where $a_K = 2\xi/\hat{\omega}$, $\xi$ is the damping parameter, $\hat{\omega} = \frac{2}{3}(2\pi/T_1)$, $R_{sy,j}$ is the yield strength of the shear spring in story *j*, and $\dot{x}_{rel,o}(t)$ is taken as zero. The sign of $R_{d,j}(t)$ is chosen so that this force opposes the shearing velocity of the story. For a low level of excitation, the building will respond as if it had linear stiffness-proportional damping, i.e., $[C] = a_K[K]$ with $[K]$ computed using the initial stiffnesses of the story shear springs. At

higher levels of excitation, the story damping forces will be capped by the $2\xi R_{sy,j}$ term, so the damping becomes nonlinear. The $2\xi$ multiplier comes from the fact that, with $a_K$ computed as $2\xi/\hat{\omega}$, the peak damping shear force in a story equals $2\xi$ times the peak shear-spring force in that story when the building undergoes harmonic linear response at the frequency $\hat{\omega}$. So, with $\xi$ =0.05 as taken previously, the damping force in each story will be capped at 10% of the shear-spring yield strength of that story. This seems like a reasonable limit to place on the damping forces.

The previous 10-story building example is now repeated with all mass, stiffness and strength parameters as before, but with capped viscous damping at $\xi$ = 0.05. Figure 11 corresponds to Figure 6 and shows the time history of the capped viscous damping force in the first story along with the time history of the shear-spring force there. The capping of the damping force at 0.10 of the shear-spring yield strength is evident. This reduction in the damping force leads to a higher first story displacement, which is reflected by an increase in the post-yield force in the shear spring (compare to the spring force in Figure 6). The displacement time histories of all ten floor levels of the building are shown in Figure 12 for two cases: linear viscous damping (the previous case) on the top and capped viscous damping on the bottom. The plotted displacements are relative to the ground. Large increases occur in the shearing displacements of the first three stories of the building when capped viscous damping is used. For the first, second and third stories, peak shearing displacements are 12.2 *cm*, 8.2 *cm* and 6.0 *cm* for the linear damping case and 16.9 *cm*, 12.6 *cm* and 9.5 *cm* for the capped viscous damping case. These significant increases demonstrate that the unrealistically high linear viscous damping forces generated by the Rayleigh damping matrix produce very unconservative results.

The concept of capped viscous damping can be generalized to more complex systems. In solid mechanics where stress and strain are used, the mass-proportional term $a_M \rho \dot{u}_i$ in equation (7) would be dropped, and bounds would be placed on the stiffness-proportional damping stresses given by the $a_K K_{ijkl} \dot{\varepsilon}_{kl}$ term in equation (8). For a situation where plastic yielding is the dominant nonlinear mechanism, appropriate caps could be based on the yield strengths of the material scaled down by the $2\xi$ factor. With other types of nonlinearity, such as interfaces where opening, closing and sliding occur, the choice of appropriate caps for the damping stresses is less obvious. For example, the sliding strength of the interface depends on the instantaneous value of the normal stress, which could vary within a wide range, including being zero when separation occurs. Such issues, as well as other damping formulations that overcome the problems demonstrated in the previous sections, are the subject of continuing investigation.

One of these potential damping formulations that is sometimes employed is to use the current tangent stiffness matrix in the stiffness-proportional part of the Rayleigh damping matrix. This will reduce the damping forces when the tangent stiffness reduces during yielding, sliding, opening, etc., which would seem to alleviate some of the problems discussed in this paper that occur when stiffness-proportional damping uses the

initial linear stiffness matrix. However, use of the tangent stiffness is an ad hoc approach since there is no physical basis to such a damping mechanism. Furthermore, the damping forces can change rapidly in time and even be discontinuous when there is a sudden change in tangent stiffness. For the example of the cracked gravity dam discussed earlier, during crack closing the damping stress $\sigma_{d,n}$ would jump from zero to a possibly large value, dependent on the closing velocity, as soon as contact is made. Such behavior can cause convergence difficulties. Use of the tangent stiffness matrix in the damping formulation is not recommended.

## CONCLUSIONS

The use of Rayleigh damping in finite element analyses of structures under dynamic loads can result in damping forces that, under certain conditions, are unrealistically large and, thus, unconservative. Assessment of these damping forces is aided by a physical interpretation of the mass and stiffness-proportional parts of the damping matrix.

The mass-proportional part of Rayleigh damping corresponds physically to linear viscous dampers that connect degrees of freedom of the structure to external supports. Although such a mechanism can not possibly exist, mass-proportional damping is commonly included in dynamic analyses because of the increased control it allows over modal damping ratios. However, problems can occur. Formulation of an earthquake analysis in terms of total motion involves a component of rigid body motion that generates extraneous damping forces if mass-proportional damping is present. An alternate formulation using motion relative to the ground solves this problem. Another example occurs in analysis of a base-isolated structure if the Rayleigh damping matrix is constructed using properties of the relatively stiff superstructure alone. The damping ratio imparted to the overall structure consisting of the superstructure and the flexible isolators can be very high owing to the mass-proportional damping term. A third type of problem arises if a portion of a structure breaks loose and thereby develops a high velocity; in which case, large mass-proportional damping forces can also develop. An example of this is a structure sliding on its base such as a concrete gravity dam. Quantification of the undesirable effects in all of these cases is detailed in the paper.

The stiffness-proportional part of Rayleigh damping corresponds physically to linear viscous dampers that interconnect the degrees of freedom of a structure. In a nonlinear analysis where the nonlinearity is of the softening type, limits on the restoring forces are imposed by various mechanisms such as yielding, cracking, sliding and buckling. If the initial linear stiffness matrix is employed to construct the stiffness-proportional damping term., then the damping forces in a softening element can reach unrealistically high values compared to the element's restoring forces as the velocity gradient across the softening element increases. The greater the initial stiffness of the softening element and the higher the velocity gradient, the greater is the effect. As quantified in the paper, this effect can be very significant.

One suggested remedy to the problems with Rayleigh damping is to eliminate the mass proportional damping contribution and bound the stiffness-proportional damping contribution. This keeps the damping forces within reasonable limits set by the analyst. In some situations, such as nonlinear contact, appropriate cap values may not be obvious. Formulation of damping strategies that ensure reasonable damping forces for a wide variety of nonlinear structural behavior is an area that needs further research.

## REFERENCES


1. Bathe K-J. *Finite Element Procedures*; Prentice Hall: New Jersey, 1996.

2. Chopra AK. *Dynamics of Structures – Theory and Applications to Earthquake Engineering*, 2nd edn; Prentice Hall: New Jersey, 2001.

3. Weaver W, Johnston PR. *Structural Dynamics by Finite Elements*; Prentice Hall: New Jersey, 1987.

4. Fung YC. *A First Course in Continuum Mechanics*; Prentice Hall: New Jersey, 1969.

5. Hall JF, Ryan KL. Isolated buildings and the 1997 UBC near-source factors; *Earthquake Spectra* 2000; **16**: 393-411.

6. Fenves G, Chopra AK. Simplified analysis for earthquake resistant design of concrete gravity dams; Report UCB/EERC-85/10, Earthquake Engineering Research Center; University of California, Berkeley; June 1986.

7. Chavez JW, Fenves GL. Earthquake analysis and response of concrete gravity dams including base sliding; Report UCB/EERC-93/07, Earthquake Engineering Research Center; University of California, Berkeley; December 1993.

8. El-Aidi B, Hall JF. Non-linear earthquake response of concrete gravity dams part 2: behavior; *Earthquake Engineering and Structural Dynamics* 1989; **18**: 853-865.


## FIGURE CAPTIONS

Figure 1. Actual damping ratio $\xi_i$ of mode *i* as a function of frequency $\omega_i$ of mode *i* when $[C]$ is given by equation (2).

Figure 2. Two formulations to implement earthquake excitation.

Figure 3. Ten-story building shown with the force-displacement relation for a typical story: $x_{j,rel}(t)$ = displacement of floor *j*; *m* = floor mass; $k_j$ = initial shear stiffness of story *j*; $R_{s,j}$ = restoring shear force in story *j*; $R_{sy,j}$ = yield value of restoring shear force;

$\Delta_j$ = displacement of story *j* (difference of floor displacements above and below). The story values are scaled to compute the $k_j$ and $R_{sy,j}$ values.

Figure 4. Top: displacement, velocity and acceleration time histories recorded at the Olive View Hospital free-field site during the 1994 Northridge earthquake. Bottom: pseudo-acceleration (light gray) and displacement (dark gray) response spectra at 5% damping.

Figure 5. Time histories of the shear-spring force in the first story (solid) and the total damping force on the building (dashed) for the Olive View ground motion scaled by 0.15 (linear response). The forces are normalized by the yield strength of the first story.

Figure 6. Time histories of the shear-spring force in the first story (solid) and the total damping force on the building (dashed) for the full-scale Olive View ground motion (nonlinear response). The forces are normalized by the yield strength of the first story.

Figure 7. Base-isolated building.

Figure 8. Force-displacement relation for the isolation system (all isolators together): $R_I$ = restoring shear force of the isolation system; $R_{Iy}$ = yield value of the restoring shear force; $D_D$ = isolator design displacement; $k_I$ = secant shear stiffness of the isolation system when displaced at the design displacement; $k_L$ = initial shear stiffness of the isolation system.

Figure 9. Concrete gravity dam that slides along a pre-existing crack through the bottom layer of finite elements.

.

Figure 10. Force-displacement (or moment-rotation) relation of high-stiffness penalty springs: $R_a$, $\Delta_a$, $k_a$ = force, displacement, stiffness of an axial spring; $R_s$, $\Delta_s$, $k_s$ = frictional force, sliding displacement, stiffness of a shear spring; $\mu$ = coefficient of friction; $M$, $\theta$, $k_r$ = plastic hinge moment, rotation, stiffness of a rotational spring; $M_P$ = plastic moment capacity.

Figure 11. Time histories of the shear-spring force in the first story (solid) and the damping shear force in the first story (dashed) for the full-scale Olive View ground motion (nonlinear response). The forces are normalized by the yield strength of the first story. These results are for capped viscous damping.

Figure 12. Time histories of displacements of the floors of the 10-story building for the full-scale Olive View ground motion (nonlinear response). The top plot is for linear viscous damping, and the bottom plot is for capped viscous damping. The ten curves in each plot correspond to the ten floor levels of the building and are motions relative to the ground.

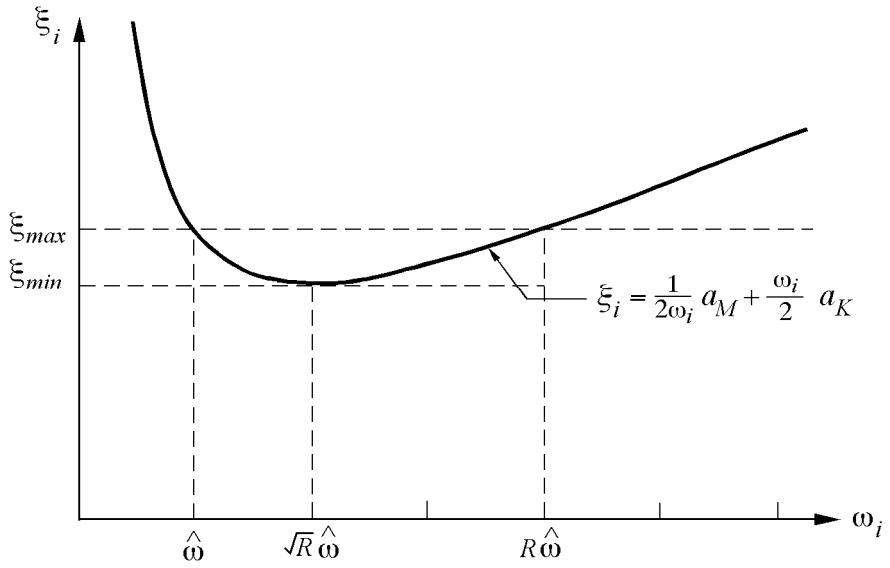


Figure 1. Actual damping ratio $\xi_i$ of mode *i* as a function of frequency $\omega_i$ of mode *i* when $[C]$ is given by equation (2).

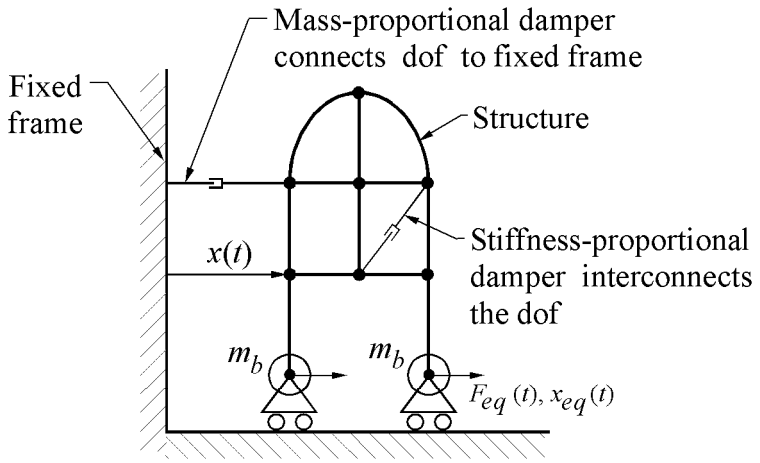


a. Structural motions $\{x(t)\}$ relative to fixed frame are computed

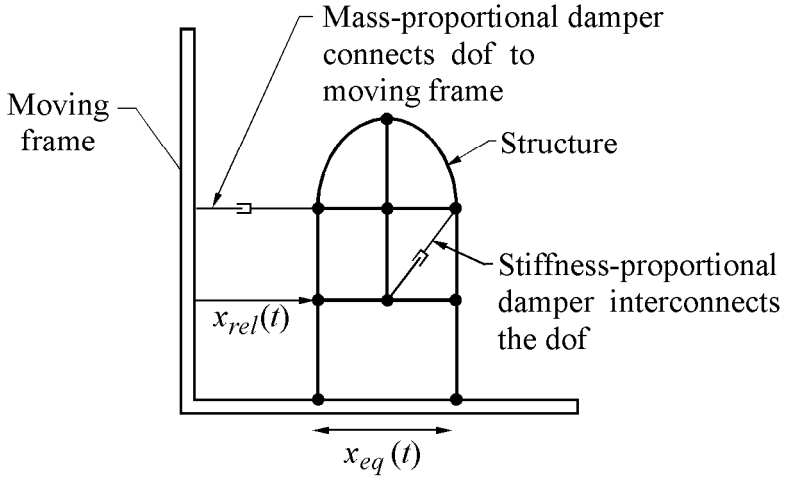


b. Structural motions $\{x_{rel}(t)\}$ relative to moving frame are computed

Figure 2. Two formulations to implement earthquake excitation.

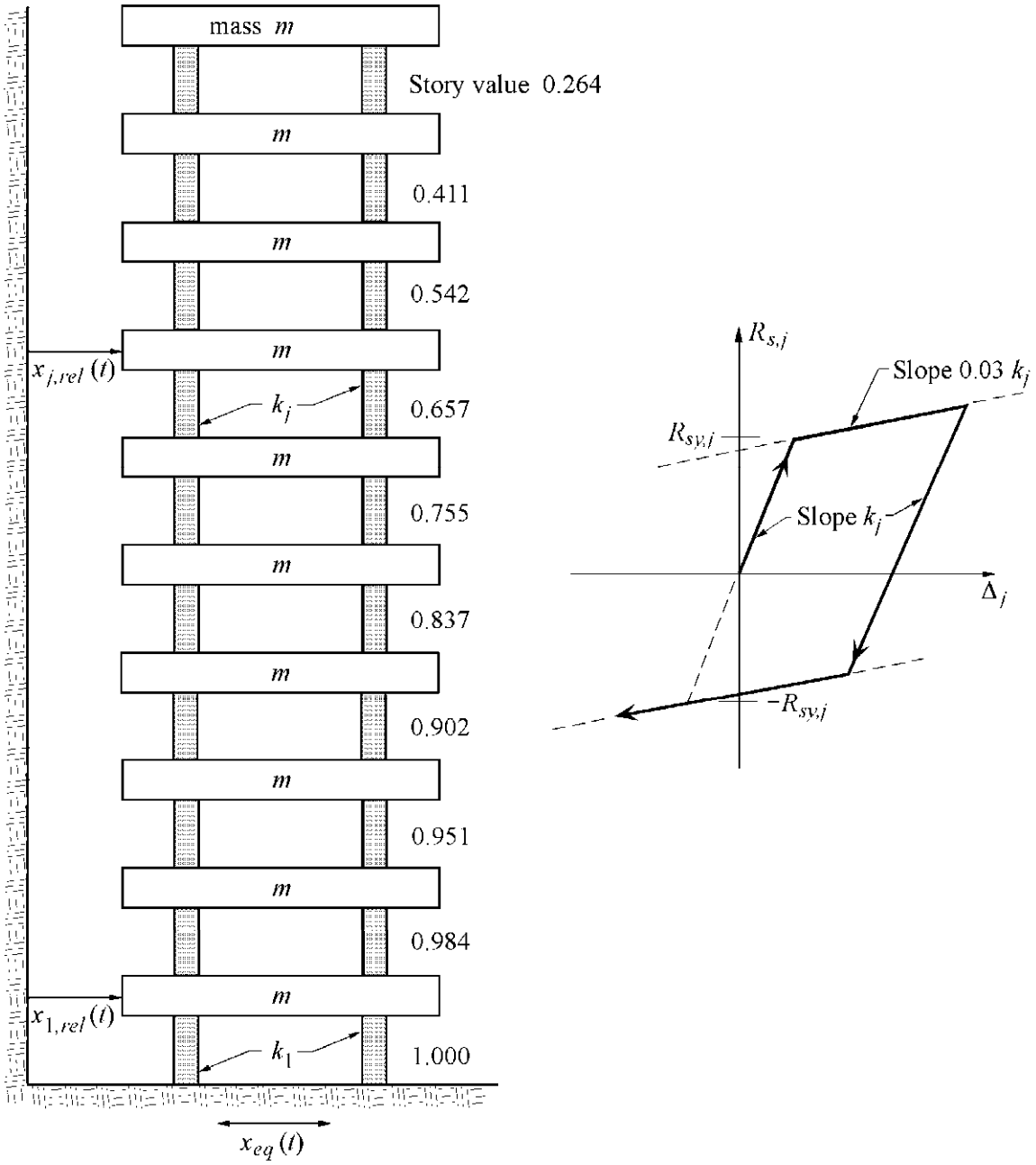


Figure 3. Ten-story building shown with the force-displacement relation for a typical story: $x_{j,rel}(t)$ = displacement of floor *j*; *m* = floor mass; $k_j$ = initial shear stiffness of story *j*; $R_{s,j}$ = restoring shear force in story *j*; $R_{sy,j}$ = yield value of restoring shear force; $\Delta_j$ = displacement of story *j* (difference of floor displacements above and below). The story values are scaled to compute the $k_j$ and $R_{sy,j}$ values.

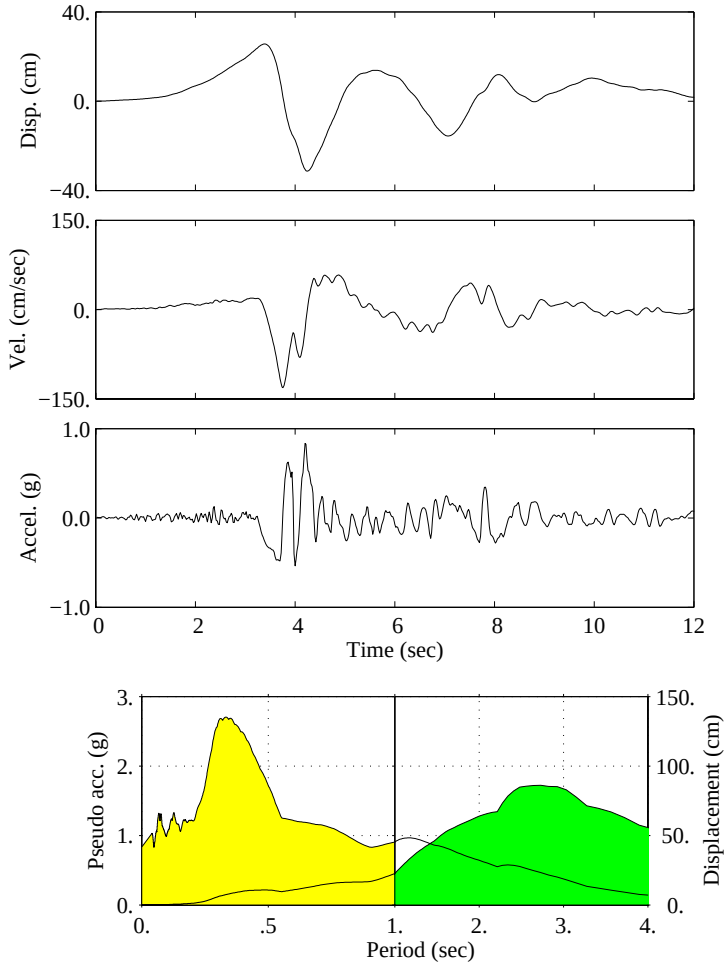


Figure 4. Top: displacement, velocity and acceleration time histories recorded at the Olive View Hospital free-field site during the 1994 Northridge earthquake. Bottom: pseudo-acceleration (light gray) and displacement (dark gray) response spectra at 5% damping.

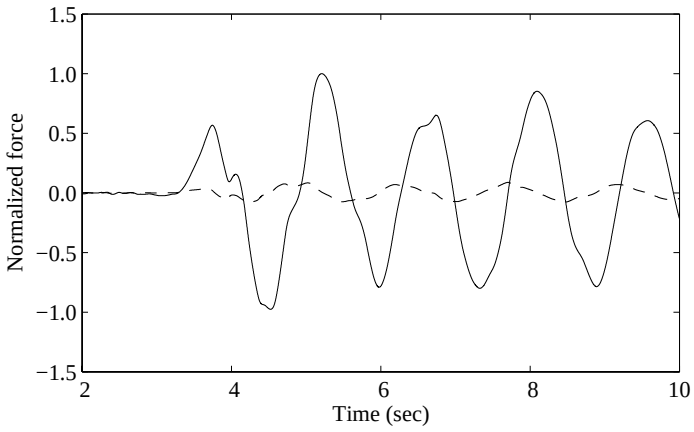


Figure 5. Time histories of the shear-spring force in the first story (solid) and the total damping force on the building (dashed) for the Olive View ground motion scaled by 0.15 (linear response). The forces are normalized by the yield strength of the first story.

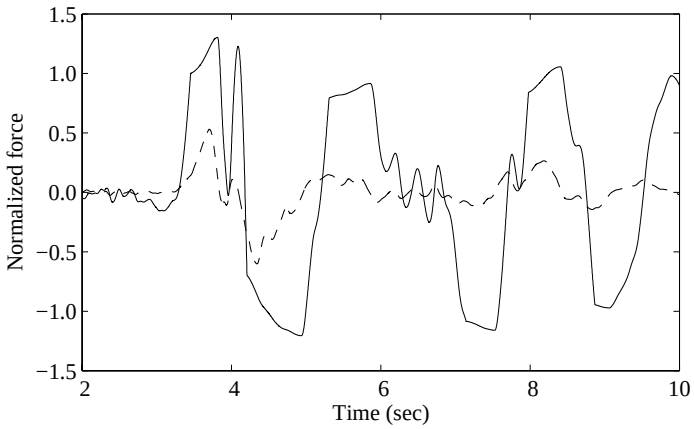


Figure 6. Time histories of the shear-spring force in the first story (solid) and the total damping force on the building (dashed) for the full-scale Olive View ground motion (nonlinear response). The forces are normalized by the yield strength of the first story.

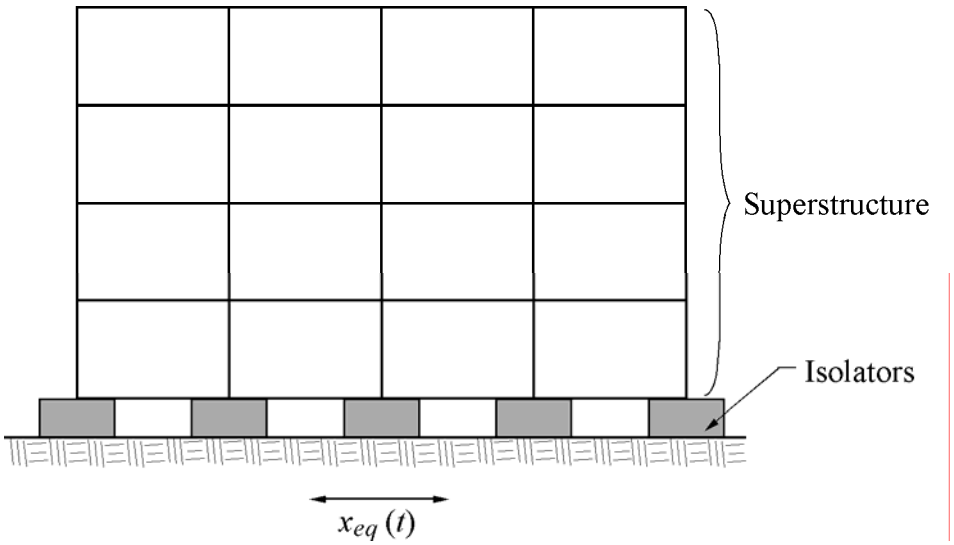


Figure 7. Base-isolated building.

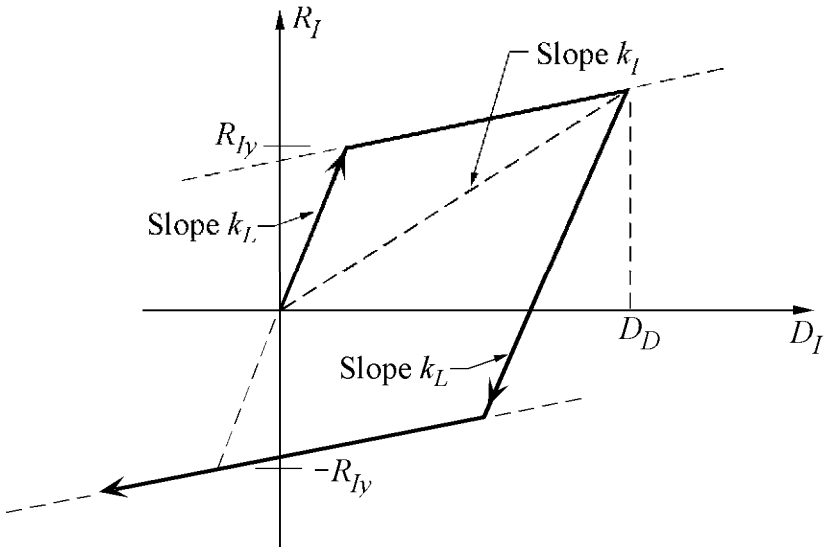


Figure 8. Force-displacement relation for the isolation system (all isolators together): $R_I$ = restoring shear force of the isolation system; $R_{Iy}$ = yield value of the restoring shear force; $D_D$ = isolator design displacement; $k_I$ = secant shear stiffness of the isolation system when displaced at the design displacement; $k_L$ = initial shear stiffness of the isolation system.

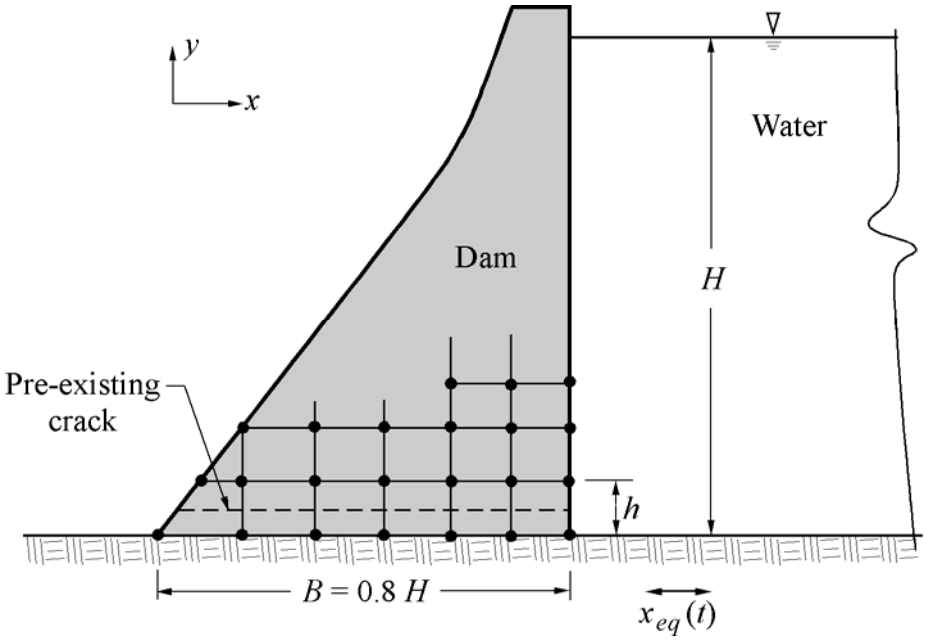


Figure 9. Concrete gravity dam that slides along a pre-existing crack through the bottom layer of finite elements.

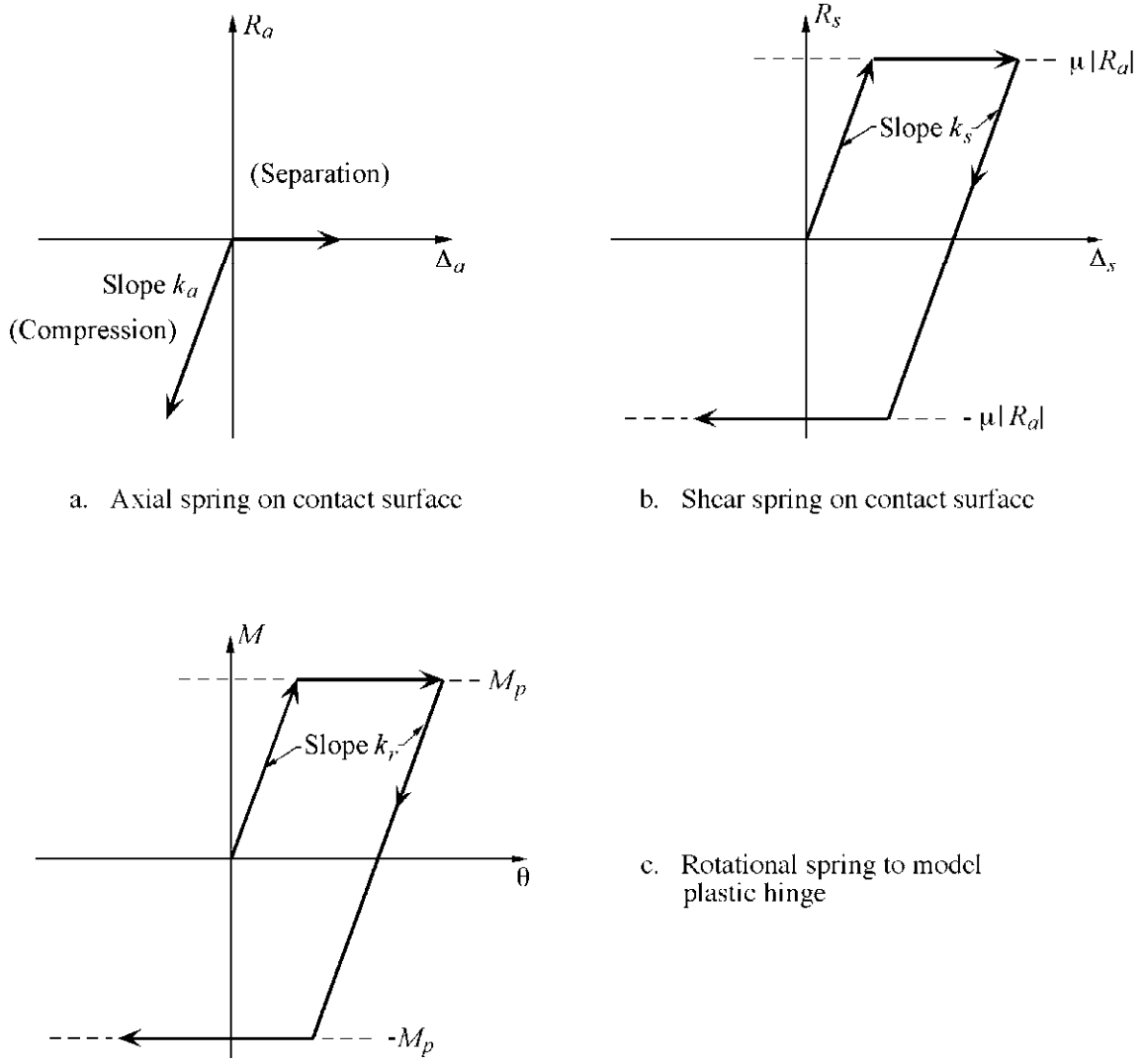


Figure 10. Force-displacement (or moment-rotation) relation of high-stiffness penalty springs: $R_a$, $\Delta_a$, $k_a$ = force, displacement, stiffness of an axial spring; $R_s$, $\Delta_s$, $k_s$ = frictional force, sliding displacement, stiffness of a shear spring; $\mu$ = coefficient of friction; $M$, $\theta$, $k_r$ = plastic hinge moment, rotation, stiffness of a rotational spring; $M_P$ = plastic moment capacity.

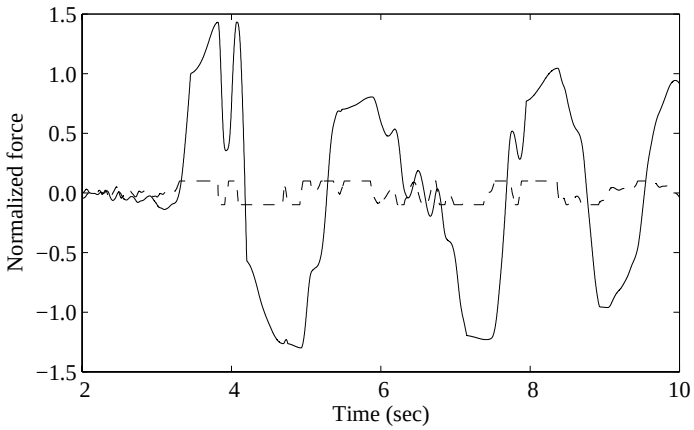


Figure 11. Time histories of the shear-spring force in the first story (solid) and the damping shear force in the first story (dashed) for the full-scale Olive View ground motion (nonlinear response). The forces are normalized by the yield strength of the first story. These results are for capped viscous damping.

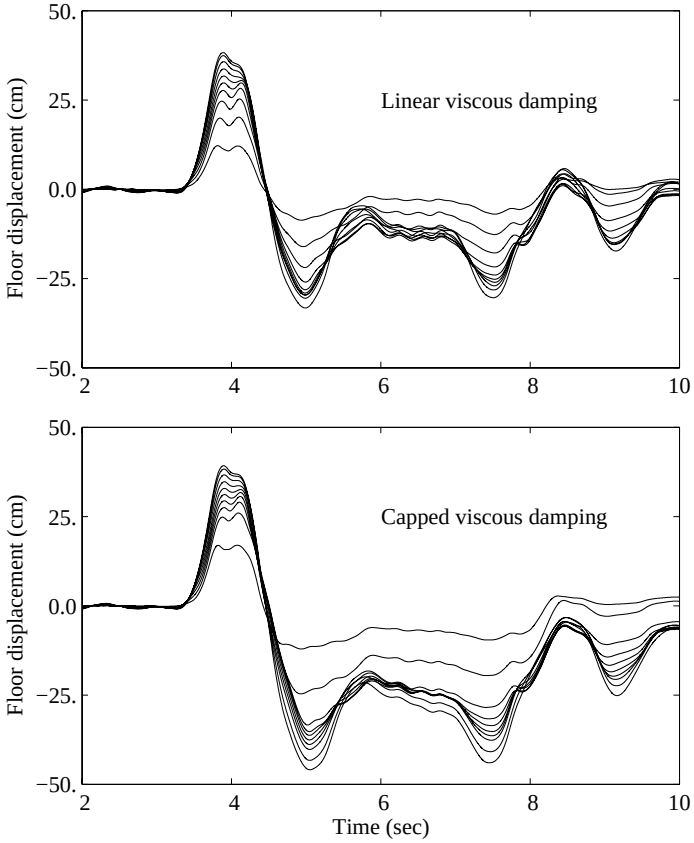


Figure 12. Time histories of displacements of the floors of the 10-story building for the full-scale Olive View ground motion (nonlinear response). The top plot is for linear viscous damping, and the bottom plot is for capped viscous damping. The ten curves in each plot correspond to the ten floor levels of the building and are motions relative to the ground.